Supporting Information

Photo-patterning and Electrochemical Energy Storage Properties of an On-chip Organic Radical Microbattery

Synthesis of PTMA.

To a mixture of 2,2,6,6-tetramethylpiperidine methacrylate monomer (9 g, 40 mmol) and 2,2'-azobisisobutyronitrile (AIBN) (0.16 g, 0.96 mmol) in 48 mL of acetic acid. The mixture was stirred at 65 °C for 12 h under N_2 atmosphere. The reaction mixture was precipitated from 200 mL of ethyl ether and treated with base, the product poly(2,2,6,6-tetramethyl-4-piperidyl methacrylate) (8.55 g, 95% yield) was obtained by filtration. To a solution of poly(2,2,6,6-tetramethyl-4-piperidyl methacrylate) (1.0 g 8.3mmol) in 20 mL methanol, $Na_2WO_4 \cdot 2H_2O$ (0.3 g, 0.9 mmol), ethylenediaminetetraacetic acid (EDTA) (0.2 g, 0.68 mmol), 30% H_2O_2 (2 mL) and H_2O (10 mL) were added and stirred at 60 °C for 48 h. PTMA was precipitated during the reaction, and the mixture was filtrated and washed with H_2O and ethyl ether to afford PTMA as a pale red solid (1.0 g, 95% yield).

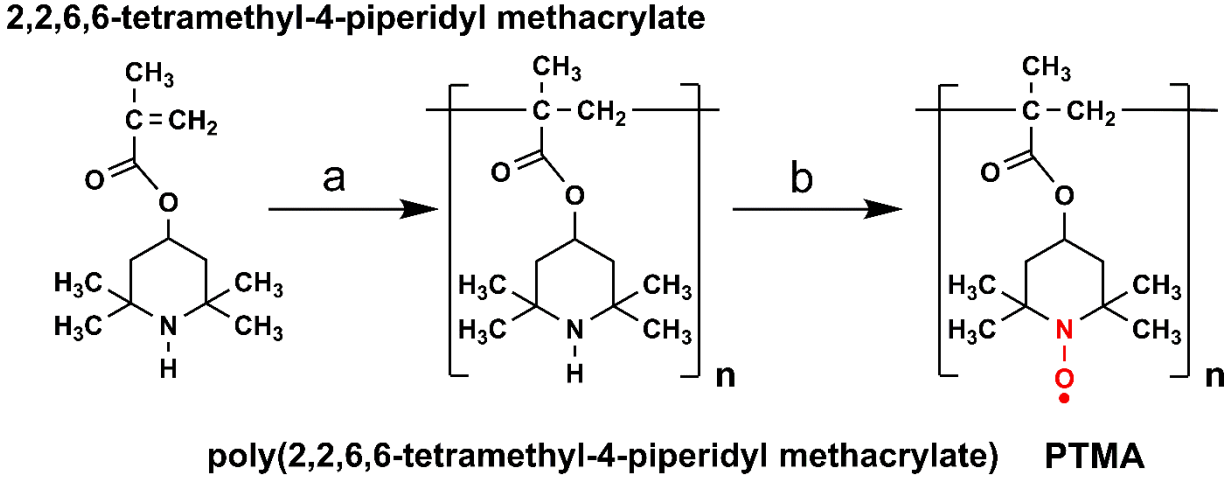

Figure S1. Synthetic schemes of PTMA: (a) radical polymerization, AIBN, 65 °C, 12 hours, (b) oxidation, H_2O_2/$NaWO_4$/EDTA, 60°C, 48 hours.

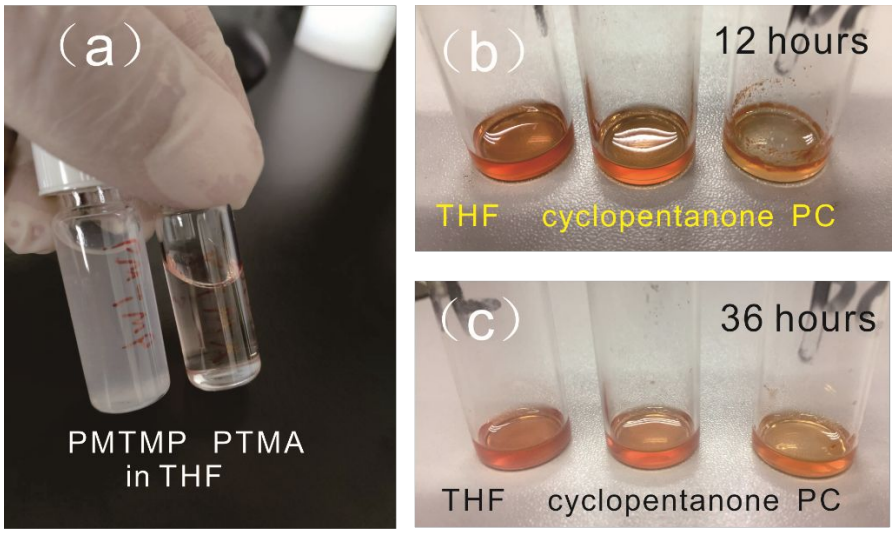

Figure S2. Solubility of PTMA. (a) Samples for GPC measurements, PTMA is soluble in THF, but the polymer intermediates PMTMP is not soluble in THF; (b-c) PTMA is well soluble in THF and the solvents for SU8 resist: cyclopentanone after ultrasonic treatment, it is only partially soluble in PC electrolyte 12 hours after a ultrasonic mixing (10 min), but well soluble after 36 hours.

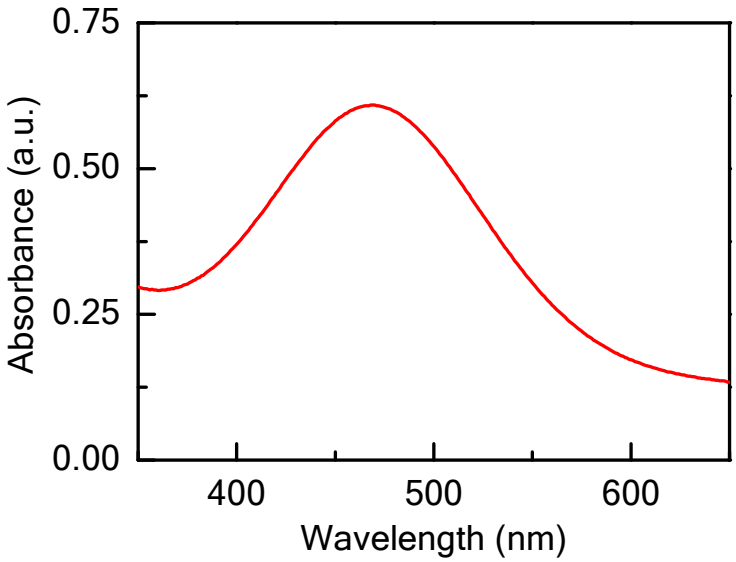

Figure S3. UV−vis spectrum of PTMA inTHF at a solution concentration of 10 mg mL^{-1}.

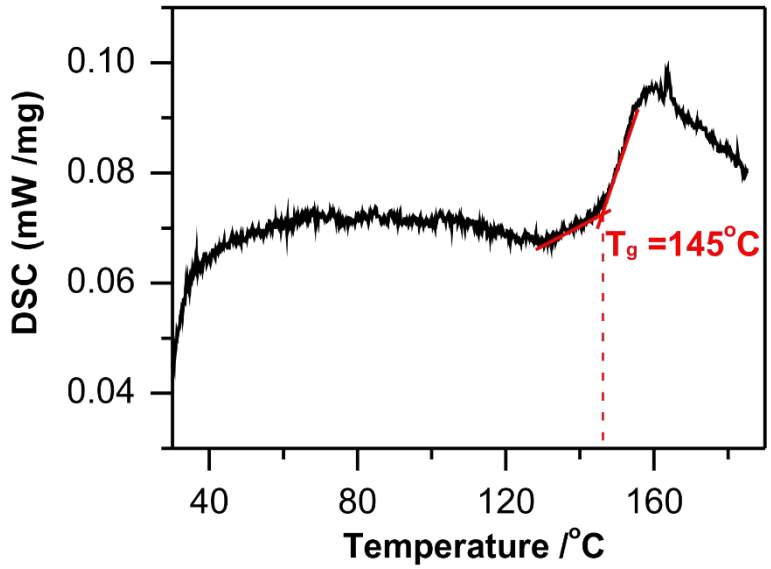

Figure S4. Measurement of T_g of PTMA by differential scanning calorimetry. The sample is first heated from r.t. to 200 °C and cooled with 10 K·min^{-1} and then heated with that same speed, the spectrum is recorded in the second heating process.

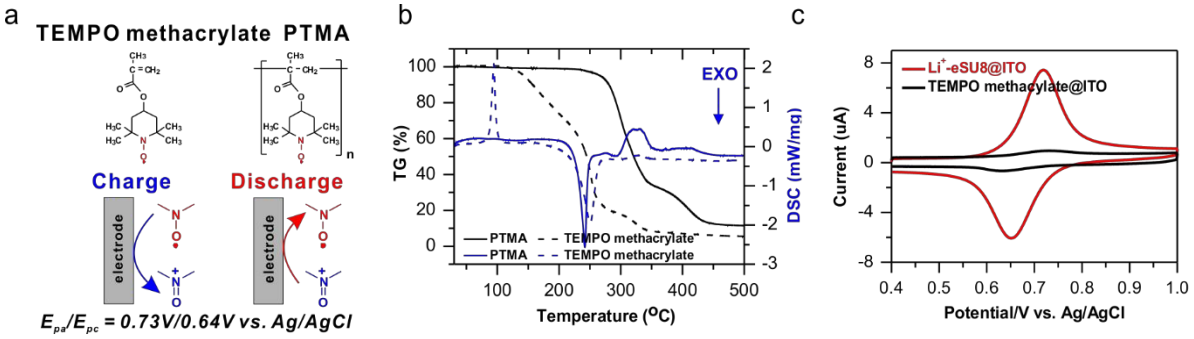

Figure S5. Property comparison of TEMPO radicals in their small molecular (TEMPO methacrylate) and polymer forms (PTMA). (a) Chemical structures of TEMPO methacrylate and PTMA , and their redox reaction in the charge/discharge process; (b) Thermogravimetry and DSC curves for TEMPO methacrylate and PTMA heated from r.t. to 500 °C in argon at 10 $K \cdot min^{-1}$. The melting point of TEMPO methacrylate is observed at ca. 95 °C with a sharp endothermic peak in DSC curve, and it starts to decompose at ca. 130 °C. Better thermal stability is found for the radical polymer PTMA, with no obvious melting point, and the polymer starts to decompose at 240 °C. (c) Cyclic voltammograms of a 5 mm×5 mm×5.6 μm TEMPO methacrylate@ITO electrode (15 wt% TEMPO methacrylate and 0.2 M $LiClO_4$ in SU8), and a 5 mm×5 mm×2.5 μm Li^+-*e*SU8@ITO electrode, recorded in 1 M $LiClO_4$/PC, at a sweep rate of v = 50 $mV \cdot s^{-1}$. Half-wave potentials ($E_{1/2}$) of the two electrodes are more or less the same at 0.68 V vs. Ag/AgCl. Unfortunately, only 3 $\times 10^{-6}$ $C \cdot cm^{-2}$ electron storage ability is found for a 5.6 μm thick TEMPO methacrylate electrode calculated on the basis of cathodic peak area of CV, which doesn't match the equivalent proportion of TEMPO compound in the SU8 electrode, while that of 2.5 μm Li^+-*e*SU8 electrode is ca. 3.5×10^{-5} $C \cdot cm^{-2}$. The low capacity can be ascribed to the good solubility of small molecular radicals, the electrode may lose majority of its electroactive compound, TEMPO methacrylate, during the developing and electro-analysis process.

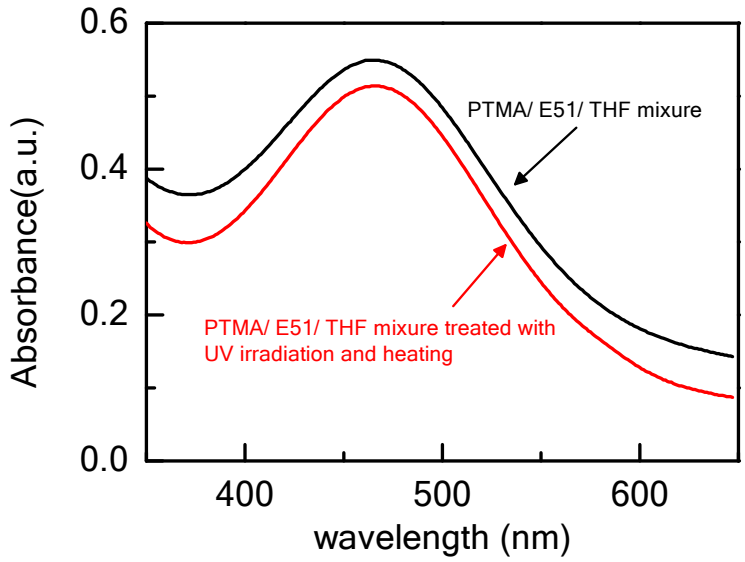

Figure S6. UV−vis spectra of PTMA/ epoxy resin E51(Nantong Xingchen Synthetic Material Co., Ltd , Epoxy equivalent g / eq: 185-188) / THF mixture before (black line) and after (red line) UV irradiation and heating, suggesting no reaction of PTMA with epoxide groups, as no obvious absorbance changes of PTMA was observed. Experimental details: PTMA (10 mg mL^{-1}) and E51 (90 mg mL^{-1}) were dissolved in THF, the mixture was examined for a UV−vis absorption spectrum. The THF solvent was completely removed under 70 ^{o}C, then exposed in Rayven UV curing oven at 2100 mJ $\cdot cm^{-2}$, and heating at 95 ^{o}C for 5 min. The obtained mixture was dissolved again in THF to reach a PTMA concentration of 10 mg mL^{-1} and a E51 concentration of 90 mg mL^{-1}, and examined for a UV−vis absorption spectrum.

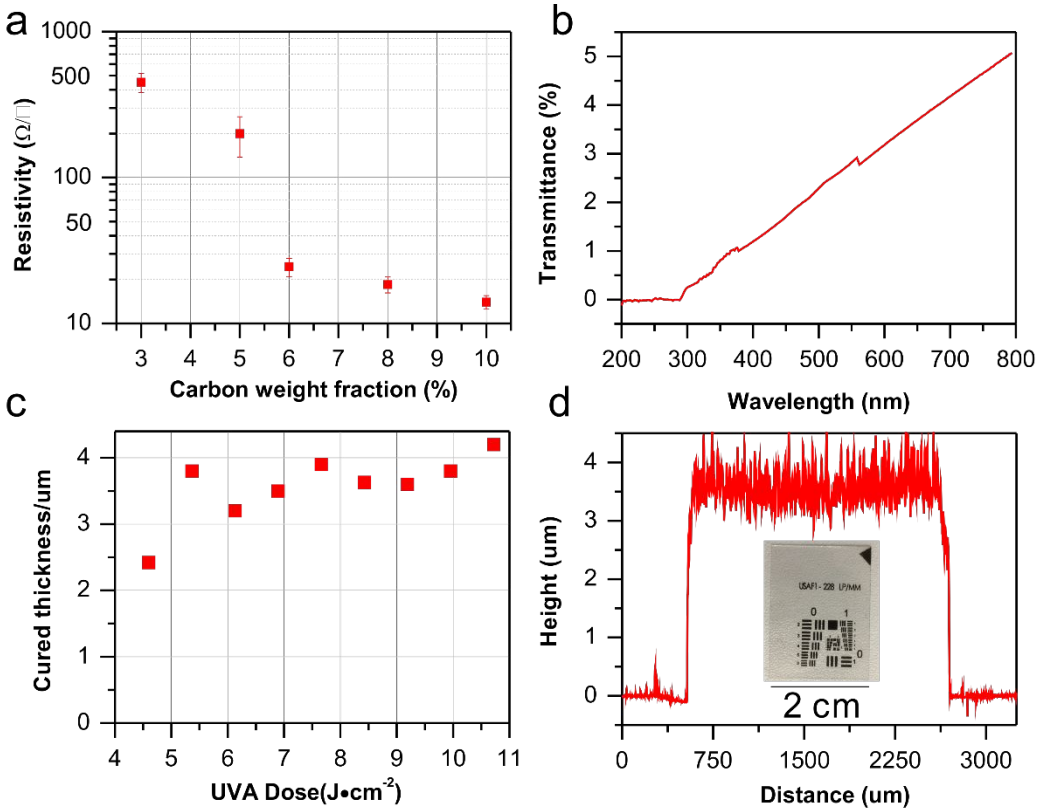

Figure S7. We try to explain one example that carbon black is added to SU8 in order to improve the electric conductivity, but lithography resolution is hampered. The extra addition of carbon black is the most common method employed in today's Lithium battery work. We add 3–10 wt% of carbon black (black pearls® 2000, CABOT) into Microchem SU8 photoresist, and mix the composite quite well using ball-milling method. (a) Resistivity of the SU8 film as a function of carbon weight fraction in the composite. Resistivity of 25 Ω/□was obtained when the loading of carbon black excess a critical value of 6 wt%. (b) Transmittance spectrum of a crosslinked SU8 film (ca. 4 μm thick) containing 6 wt% carbon black, less than 1% transmittance was obtained at the UV irradiation range. (c) Cured thickness of carbon black modified SU8 film as a function of UVA energy, back-side irradiation was used to study the influence of irradiation energy on photo-polymerization of the composite resists, the thickness of the structure obtained after development corresponded to the cured depth. However, cured thickness of lower than 4 μm can only be achieved even when the UV expose dose was bigger than 10 $J \cdot cm^{-2}$, because of the low transmittance at the exposure wavelength (less than 1%,). (d) Optical image of a photopatterned structure, and the profile of the thickness of structure.

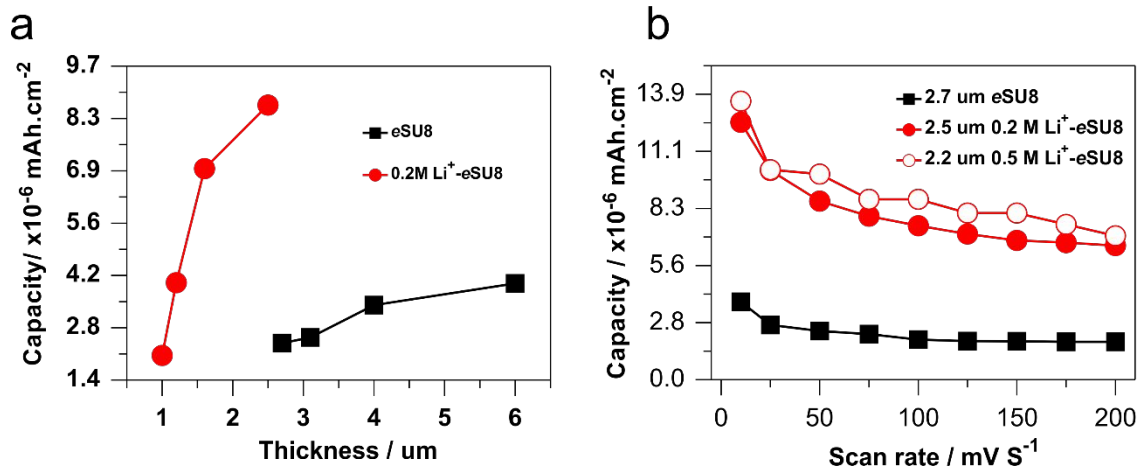

Figure S8. (a) Areal capacity of *e*SU8 (black line) and Li^+-*e*SU8 (red line) as a function of film thickness, the capacity was calculated on the basis of cathodic peak areas of CVs at v = 50 mV s^{-1}; For *e*SU8 electrode, the capacity is generally proportional to its thickness, but the capacity grows sharply with its thickness after the addition of $LiClO_4$ salts. (b) Areal capacity of *e*SU8 and Li^+-*e*SU8 as a function of sweep rate in the range of 10 mv.s^{-1} to 200 mv.s^{-1}.

Quasi-reversible redox of Li$^+$-*e*SU8.

For Li$^+$-*e*SU8 electrodes, it is noted that the difference of separation of the anodic ($\mathbf{E_{ap}}$: 0.70 V) and cathodic ($\mathbf{E_{cp}}$: 0.66 V) peak potentials, ΔE_p, is estimated as 0.04 V at a sweep rate of 10 mV/s, and the ΔE_p grows to 0.17 mV with the increment of sweep rate from 10 mV/s to 200 mV/s (**Figure S9**, **Table S1**). The small ΔE_p corresponds with its fast electrode reaction rate of the present polymer radicals, which leads to a capability for high power rate in the charge and discharge process of the battery. Both of the anodic and cathodic peak currents show approximately proportional to the sweep rate over the range of 10−200 mV·S^{-1}, and the Li$^+$-*e*SU8 films exhibit the typical behaviour anticipated for a surface-confined redox couple with a small ΔE_p value, suggesting that the redox process is surface-confined. The areal capacity of the Li$^+$-*e*SU8 is steady decreased with the increment of sweeping rate from 10 to 200 mV·S^{-1}, i.e., 1.4×10^{-5} mAh·cm^{-2} @10 mV·S^{-1}, 1.0×10^{-5} mAh·cm^{-2} @50 mV·S^{-1}, 7.8×10^{-6} mAh·cm^{-2} @100 mV·S^{-1}, 7.0×10^{-6} C·cm^{-2} @200 mV·S^{-1}. Thus, the electrochemical behaviour of the Li$^+$-*e*SU8 electrode can be considered as a quasi-reversible process.

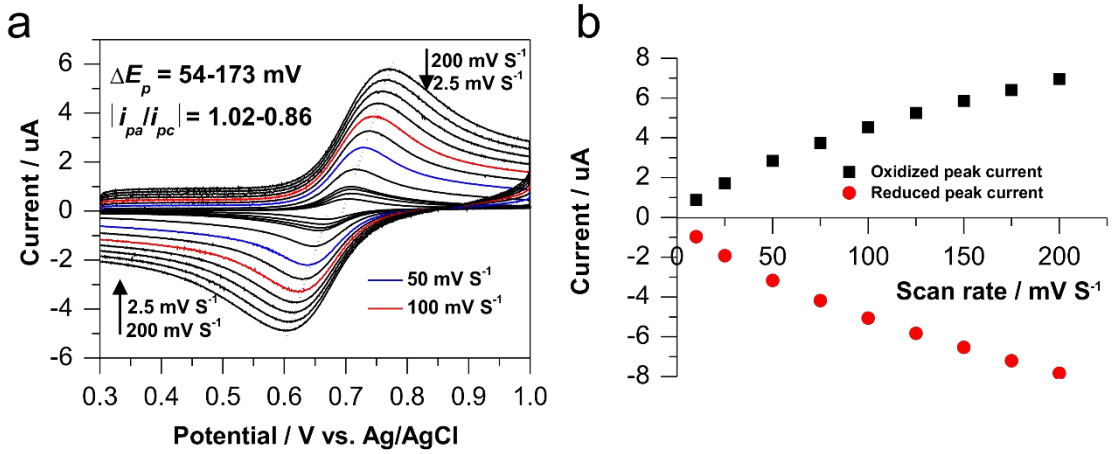

Figure S9. (a) CV of a Li$^+$-*e*SU8 electrode at a sweep rate in the range of 2.5~200 mV.s^{-1}; (b) The redox peak current of a Li$^+$-*e*SU8 electrode as a function of sweep rate.

Table S1. Electrochemical parameters of a Li^+-*e*SU8 electrode as a function of sweep rate, recorded in 1 M $LiClO_4$/PC.

Sweep rate **[mV.S^{-1}]**	**E_{pa}** **[V]**	**E_{pc}** **[V]**	**ΔE_p** **[mV]**	**i_{pa}** **[µA]**	**i_{pc}** **[µA]**	**$\lvert i_{pa}/i_{pc} \rvert$**
10	0.709	0.655	54	1	0.99	1.02
25	0.713	0.648	65	1.7	1.80	0.95
50	0.729	0.637	92	2.6	2.84	0.92
75	0.738	0.627	111	3.3	3.64	0.91
100	0.752	0.623	129	3.9	4.39	0.89
125	0.754	0.62	134	4.4	5.05	0.87
150	0.761	0.609	152	4.9	5.63	0.87
175	0.77	0.604	166	5.4	6.23	0.87
200	0.772	0.599	173	5.8	6.76	0.86

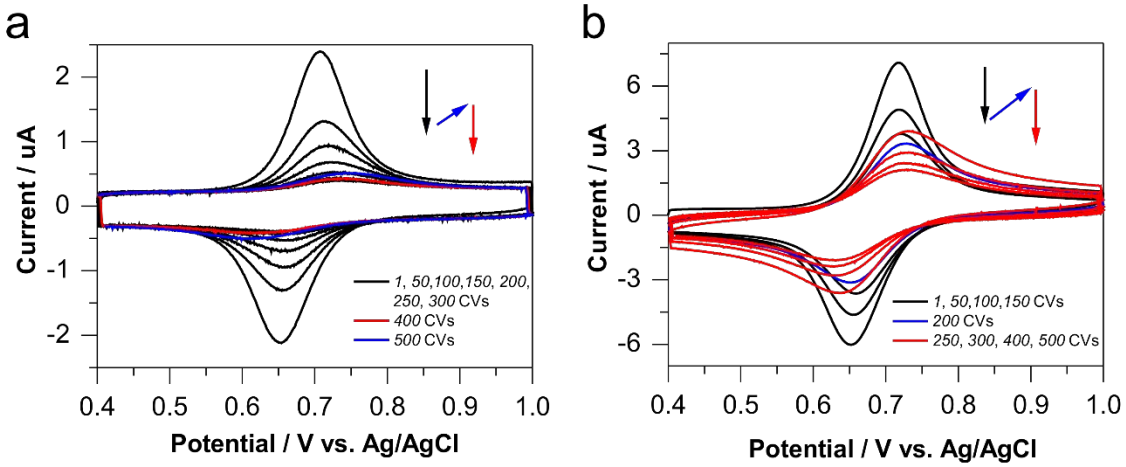

Figure S10. CVs dependence on the number of continuous cyclic potential sweeps for (a) *e*SU8 and (b) Li^+-*e*SU8 electrodes in 1 M $LiClO_4$/PC, at v = 50 mV s^{-1}. Inset: change trend in current.